Analyst

Accepted Manuscript

ROYAL SOCIETY OF CHEMISTRY

www.rsc.org/analyst

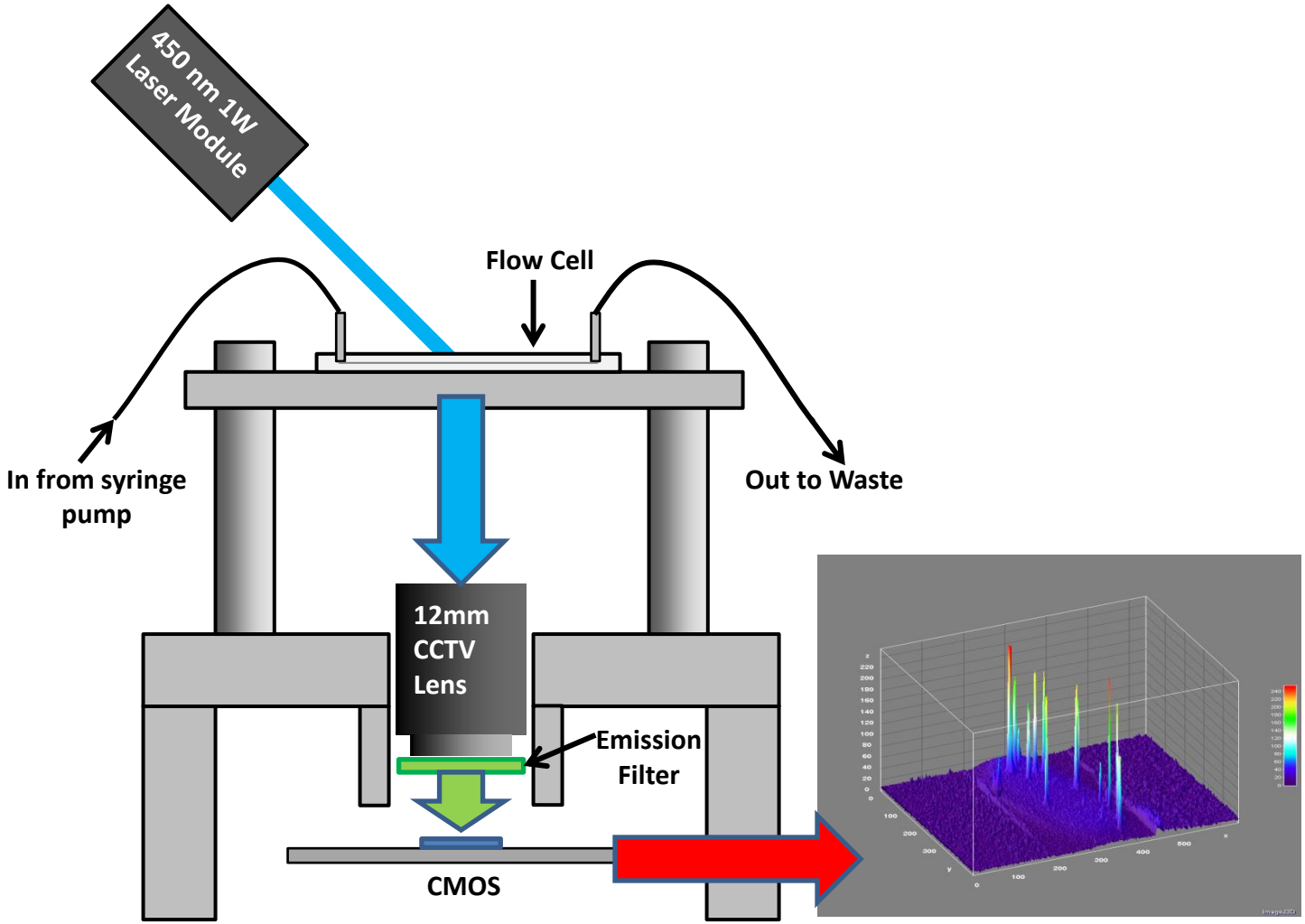

Webcam-based flow cytometer using wide-field imaging for low cell number detection at high throughput

Joshua Balsam[1,2], Hugh Alan Bruck[2], and Avraham Rasooly[1,3]

[1]Division of Biology, Office of Science and Engineering, FDA, Silver Spring, MD 20993

[2]University of Maryland, College Park, MD 20742

[3]Division of Cancer Biology, National Cancer Institute, Rockville, MD 20850

[*]Address correspondence to: Dr. Avraham Rasooly, NIH/NCI, 9609 Medical Center Drive Rockville, MD 20850, Phone: (301) 240-276-6186 e-mail: rasoolya@mail.nih.gov

ABSTRACT

Here we describe a novel low-cost flow cytometer based on a webcam capable of low cell number detection in large volume which may overcome the limitations of current flow cytometry. Several key elements have been combined to yield both high throughput and high sensitivity. The first element is a commercially available webcam capable of 187 frames per second video capture at a resolution of 320x240 pixels. The second element in this design is a 1 W 450 nm laser module for area-excitation, which combined with the webcam allows for rapid interrogation of a flow field. The final element is a 2D flow-cell which overcomes the flow limitation of hydrodynamic focusing and allows for higher sample throughput in a wider flow field. This cell allows for the linear velocity of target cells to be lower than in a conventional "1D" hydrodynamic focusing flow-cells typically used in cytometry at similar volumetric flow rates. It also allows cells to be imaged at the full frame rate of the webcam. Using this webcam-based flow cytometer with wide-field imaging, it was confirmed that the detection of fluorescently tagged 5 μm polystyrene beads in "1D" hydrodynamic focusing flow-cells was not practical for low cell number detection due to streaking from the motion of the beads, which did not occur with the 2D flow-cell design. The sensitivity and throughput of this webcam-based flow cytometer was then investigated using THP-1 human monocytes stained with SYTO-9 florescence dye in the 2D flow-cell. The flow cytometer was found to be capable of detecting fluorescently tagged cells at concentrations as low as 1 cell/mL at flow rates of 500 μL/min in buffer and in blood. The effectiveness of detection was concentration dependent: at 100 cells/ml 84% of the cells were detected compared to microscopy, 10 cells/ml 79% detected and 1cell/ml 59% of the cells were detected. With the blood samples spiked to 100 cells/ml, average concentration for all samples was 91.4 cells/mL, with a 95% confidence interval of 86-97 cells/mL. These low cell concentrations and the large volume capabilities of the system may overcome the limitations of current cytometry, and are applicable to rare cell (such as circulating tumor cell) detection The simplicity and low cost of this device suggests that it may have a potential use in developing point-of-care clinical flow cytometry for resource-poor settings associated with global health.

Key words: mHealth, webcam, global health, cytometry, fluidics, fluorescence, low cell number detection, rare cells

1. INTRODUCTION

The main elements of flow cytometers are a fluidic system for carrying biological media and an optical system for detecting them. Most current flow cytometers utilize microfluidic sheathing and integration of optics through a technique known as "flow focusing". The sheathing is used to constrain the spatial location of cells or particle to a very narrow region so that cells can be interrogated one at a time by the narrow field detector which is based on photomultipliers or other narrow field detectors. Microflow cytometers typically used channels etched in glass or silicon, while more recently polydimethylsiloxane (PDMS) and lithography technology have also been employed to fabricate the fluidic channels quickly and inexpensively. In a recent device, passive hydrodynamic focusing generated by chevron grooves imbedded on the walls of the microchannel [1, 2] enables the sheath fluid to completely surround the sample stream. However, one limitation of the focused stream is a low flow rate due to the high hydrodynamic resistance and pressure constraints of the cell, which ultimately limits the device to small volumes or long analysis times, limiting the utility of the technology for analysis of low cell number in large sample volume. In addition to the commonly used photomultipler based detection, full-field imaging sensors can be used for detection combined with classical flow cytometry [3]. While conventional flow cytometry does not provide morphologic information of cells (other than cell size), imaging-based cytometry can provide multispectral imagery related to the cell morphology [4]. Such multispectral image cytometry has many cellular research applications ranging from analysis of protein co-localization on cells [5] to counting circulating tumor cells [6]. However, such devices are expensive, complex and are mainly used for basic biological research.

Portable cytometers are being developed for a broad variety of point-of-use applications especially for point-of-care (POC) clinical applications or environmental analysis. Because of the inherent portability of full-field imaging sensors, either complementary metal-oxide-semiconductor (CMOS) or charge-coupled device (CCD) cameras can be employed as relatively simple, low cost, sensitive devices for optical detection over large areas, and have already been employed in several array assays [7-10]. Their main advantage is they can be used for analyzing light from a large enough area that it can cover the entire surface of a lab-on-a-chip (LOC) or an

array [11-13]. This has made CMOS or CCD-based detectors an ideal choice for LOC multichannel detection, since many sample channels can be analyzed simultaneously.

Portable cytometers have potential for POC clinical applications and for use in low and middle-income countries. LOC fluidic technology provides a potential approach for developing POC analytical tools in resource-poor settings[14, 15]. Recently, optofluidic fluorescent imaging cytometry on a cell phone with a spatial resolution of ~2 μm was described [16, 17]. While very mobile and versatile, the flow rate of this system is ~1 μL/min, which limits analysis to small volumes. Mobile phones are used effectively for mobile POC devices [16-24], however the cameras in these phones are often limited in their sampling rates (e.g., many phones are limited for 30 fps) and are less versatile with their optical systems (e.g., inability to change lenses) than devices such as webcams.

The detection system described in this work is based on a fluorescence detector detecting fluorescently labeled cells. Detection of fluorescently labeled cells is a widely used technology in medical diagnostics. Cells with specific fluorescently tagged ligands can be labeled and detected by fluorescence detectors at the appropriate wavelength. This technology forms the basis for such popular techniques as FACS (Fluorescence-activated cell sorting).

Detection of fluorescently tagged cells in a device, such as the one described here, depends on many factors including the fluorophore quantum yield, excitation photon flux, performance of antibody labeling (i.e. number of fluorophores bound to each cell), and the exact optical configuration of the detector. In previous work, we demonstrated that the fluorescence detector used in this work is capable of sensitive detection of fluorescent signals [13, 25-34]. This work describes a low-cost flow cytometer based on webcam imaging that is capable of large volume analysis and low cell number detection which may overcome the limitations of current flow cytometry. The device is suitable for low resource settings in global health applications, providing both the high throughput and high sensitivity need for medical diagnostics. The flow cytometer is realized through the combination of three elements: (a) a commercially available low cost webcam for high speed imaging, (b) a commercially available laser module for area-excitation, and (c) a 2D flow-cell that allows for high sample throughput at low velocities by

using a wider flow field that overcomes the volume limitation associated with the hydrodynamics of flow focusing. The sensitivity and throughput of this new cytometer are investigated and quantified using fluorescently tagged THP-1 human monocytes stained with SYTO-9 dye. The suitability of the webcam-based flow cytometer for low cell number detection in large volume was also investigated without the 2D flow-cell in flow focusing mode to compare with the wide-field mode.

2. MATERIALS and METHODS

2.1 Flow-cells fabrication

A flow focusing cell (Figure 1) was fabricated using an Epilog Legend CO_2 65 W laser cutter (Epilog, Golden, CO) using similar techniques described in our previous work [15, 25-27, 29, 35]. The flow-cell consisted of three functional layers. The top layer consisted of a 3 mm thick clear acrylic plate (75 x 25 mm) with laser machined inlet and outlet ports into which 18GA needles were pressed and bonded to allow for sample injection and waste collection. The middle layer, which defined the shape of the fluid flow, was laser machined from a single layer of 3M 9770 double-sided adhesive transfer tape (Piedmont Plastics, Beltsville, MD), resulting in a flow-cell with width 0.2 mm, length 45 mm, and depth of approximately 0.075 mm. The bottom layer consisted of a single glass microscope slide. The wide-field cell (Figure 2) was fabricated with steps identical to those of the flow focusing cell, with the exception of the width of the middle layer. The width of this channel was 4 mm. A Fusion100 syringe pump was used for flow rate control (Chemyx, Stafford, TX).

2.2 *Webcam-based cytometer platform*

A Sony PlayStation® Eye webcam was used as the photodetector. A c-mount CCTV lens (Pentax 12 mm f/1.2) was used to replace the stock webcam lens. For florescence detection, a green emission filter with center wavelength 525 nm and bandwidth 50 nm (Chroma Technology Corp., Rockingham, VT) was used for detecting fluorescent emission. For fluorescent excitation, a 1 W 450 nm laser module was used (Hangzhou BrandNew Technology Co., Zhejiang, China). The laser illuminates the flow-cell at an angle of approximately 45º. The flow cytometer platform was constructed using 0.5 inch thick clear acrylic sheet and nylon rod (McMaster-Carr, Robbinsville, NJ).

2.3 Computer control and data analysis

The webcam sensor was connected to a 32-bit Windows-based laptop computer via a USB2 port. Drivers and software allowing the webcam to be controlled on a personal computer were developed and freely distributed by Code Laboratories, Inc. (Henderson, NV). The camera control software (CL-Eye Test) was used to set camera parameters (exposure time, frame rate, and gain) and to capture and save video in uncompressed AVI format. Video files were analyzed using ImageJ software (freely distributed by NIH, http://rsb.info.nih.gov/ij/download.htm), and data analysis and plotting was carried out in Microsoft Excel (Redmond, WA).

2.4 Cell culture and staining

Fluorescently stained THP-1 human monocytes were used to demonstrate low cell number detection. Cells were removed from an active culture, pelleted by centrifugation and resuspended in PBS. 10 μL SYTO-9 dye (5 mM stock concentration) was added to 1 mL of suspended cells and allowed to rest at room temperature in the dark for 20 minutes. Cells were then pelleted and washed three times with PBS to remove excess dye.

2.5 Low cell number preparation

The stock solution of cells after staining was diluted to a level of approximately 1 cell/μL (measured by microscopy) to allow for manual counting. Cell concentration was measured by placing 3 μL sample droplets on a microscope slide and counting cells in the droplet in real time under laser excitation using the same imaging platform employed to image the flow-cells in these experiments. This was repeated many ($N > 20$) times. An average cell concentration of 0.93 cells/μL with a standard deviation of 0.5 is an example of a typical result of these measurements. From this relatively high concentration, lower concentration samples of 100, 10, and 1 cell/mL were generated by single-step dilution. For each dilution, 107.5 μL of stock solution (with measured concentration of 0.93 cells/μL) was diluted into a volume of buffer to yield the final target concentration (1 mL, 10 mL, and 100 mL of buffer for concentrations of 100, 10 and 1 cell/mL, respectively). Based on a normal sampling distribution with standard deviation of 0.5 cells/μL, the 95% confidence range for each concentration was 90-110, 9-11, and 0.9-1.1

cells/mL for concentrations of 100, 10 and 1 cell/mL, respectively. Pipetting volume error was measured to be less than 1%.

2.6 Whole Blood Sample Preparation and Measurement

Human whole blood (single draw, O+) was purchased from BioChemed Services (Winchester, VA). 3 mL samples of whole blood was diluted 10X in 25 mM HEPES buffer for a final volume of 30 mL. THP-1 monocytes were removed from an active culture, pelleted and resuspended in 25 mM HEPES. 10 µL of 5 mM Syto-9 nucleic acid fluorescent stain (Life Technologies) was added to 1 mL of THP-1 cells and allowed to rest at room temperature in the dark for 20 minutes followed by pelleting, washing and resuspension to remove unbound dye. Cell concentration in the stock solution was determined to be 4.3 cells/µL as described above. 23 µL of the stock cell suspension was spiked into to each 30 mL diluted blood sample to yield a final concentration of 100 cells per mL of whole blood (i.e. 300 cells per 3 mL whole blood, which was diluted 10X to 30 mL). The 95% confidence level for the final concentration in each sample was 93-107 cells/mL based on 20 measurements of the stock cell suspension.

2.6 Calculated flow rate for flow focusing case

To determine the actual flow rates in the flow focusing case, individual video frames of cells flowing through the focused stream were analyzed. Based on the known geometry of the flow-cell (width X and depth Z), the measured width of the flow-cell in pixels (X_P), the measured distance moved by single cells between frames in pixels (d_Y), and exposure time (t_{EXP}), average flow rate ($\dot{V}$) could be calculated:

$$\dot{V} = \frac{\frac{X}{X_P} d_Y X Z}{t_{EXP}}$$

2.7 Low cell number counting

Cell dilutions were loaded into a 3 mL syringe and injected through the wide-field flow-cell at a rate of 500 µL/min. This was the highest flow rate that resulted in cell images which were not streaked when imaged at the maximum frame rate of the webcam sensor. Video of this flow was saved and analyzed later in ImageJ. The video files generated were typically around 10-15 GB in size, and had to be opened and analyzed in several fragments. After being opened in ImageJ,

each fragment of video was split into its three color channels (red, green, and blue). The fluorescent dye used in this case had its emission peak in the green channel, so the red and blue channels were discarded to reduce background noise.

3. RESULTS AND DISCUSSION

Current flow cytometry which is based on photomultipliers or other narrow field detectors relies on flow focusing to constrain the spatial location of cells to a very narrow region. Hydrodynamic flow focusing allows cells to be interrogated one at a time by the narrow field detector. There are several advantages to a flow focusing design. Because the path of every cell is nearly identical, the area over which laser excitation is needed is much smaller. This allows for a lower power laser to be used if it is focused onto this small area, thereby reducing power requirements and overall cost. Similarly, the narrow field detector can be focused to a point measurement. Such detection schemes are used in commercial flow cytometers which use point detectors (typically photomultiplier tubes), in this work we study the used imaging cytometry.

3.1 Imaging Flow Focusing Cytometry

The first iteration of our imaging flow cytometer platform was based on this approach, utilizing a flow-cell with flow focusing and a webcam as detector. Figure 1-I shows a schematic of the flow focusing cell. In this cell configuration there are three fluidics inlets, a sample inlet (A) and two sheath fluid inlets (B). The interrogation region for the webcam is shown at (C) and a waste outlet at (D). The schematic (Figure 1-II) and a photograph (Figure 1-III) of actual flow focusing effect using food dye for visualization shows narrow focusing (~30 μm in 150 μm channel).

One of the main limitations of this focused flow-cell fabricated by lamination is the maximum sample flow rate. We found that the maximum flow rate achievable was limited by the ability of the flow-cell to withstand pressure. The hydrodynamic resistance from the Poiseuille flow through a narrow channel of effective diameter, d, increases proportionally to $1/d^4$. In our flow-cell, leaks developed around the chip interface ports at flow rates above 100 μL/min, and the layers of the flow-cell began to delaminate.

We tested the flow focusing cell for the detection of 5 μm polystyrene beads, detected by a regular 30 fps webcam, which is the same frame rate typically used in smartphones. Even with low flow rate we were unable to image the beads due to image streaking and poor image quality. So, a webcam with a faster frame rate was employed (Sony PlayStation® Eye webcam). For a typical low cell number detection case, several milliliters of sample must be interrogated. For a 10 mL sample, a flow rate of 100 μL/min would result in a 100 minute analysis time. Even with a flow rate of 100 μL/min in our flow focusing cell, using the maximum camera frame rate of the webcam sensor we employed (187 fps) was not sufficient to capture all of the passing cells. A reduced flow rate of 10 μL/min was required because of the camera limitation (Figure 1-IV and 1-V). Even with this flow rate (which will requires 16.7 hours for 10 mL analysis) beads streaking caused by the movement of the beads in the 1/187 second was observed (Figure 1-IV and 1-V) suggesting that flow focusing combined with webcam detection is not practical for low cell number in large volume detection. It is for this reason that a non-focusing wide-field flow-cell was developed.

3.2 Webcam-based flow cytometer with wide-field imaging for high throughput low cell number in large volume detection

A wide-field flow-cell was developed in order to overcome the image streaking problems of flow focusing, to utilize the inherent wide-field imaging capability of the webcam, and to reduce the analysis time for low cell number detection.

As shown in Figure 2-A, the flow cytometer consists of four modules: a webcam sensing element, a laser excitation source, a flow-cell, and a focusing stage to hold each module in alignment and enable focusing. The sensing element consists of the internal elements of a webcam, a 12 mm f/1.2 CCTV lens, a green emission filter, and a computer to collect and analyze data. The excitation source is a 1W 450 nm laser module. The sample handling module consists of a flow-cell and a programmable syringe pump.

The flow-cell (Figure 2-B) consists of a 4 mm wide channel through which sample is injected via an inlet and collected at the outlet. For large volume analysis, the maximum flow rate achievable through this cell is 10 mL/min. However, the flow rate in experiments presented in this paper

was limited to 500 μL/min due to the maximum frame rate achievable by the webcam employed for sensing. This was done to eliminate cell image streaking. For very low cell number detection this requirement could be relaxed to allow for higher flow rates at the expense of flow resolution.

A challenge inherent in fluorescent imaging of a wide-field flow-cell is the excitation source. In this case, a 1 W consumer laser was used to project an elliptical spot which covered the width of the flow-cell. A laser such as this is fairly expensive (~$300) for a device designed for use in a low-resource setting. To reduce the cost of the laser, a lower power laser with line generator optics could be used to further focus the laser spot. This could allow the critical parameter of photon flux to remain unchanged while reducing overall power.

A Sony PlayStation® Eye webcam was used as the photodetector in this platform by converting the webcam to a microscope. The device was disassembled and the main circuit board (with attached image sensor and USB cable) was removed. The circuit board was incorporated directly into the flow cytometer platform, and a C-mount CCTV lens (Pentax 12 mm f/1.2) was used to replace the stock webcam lens in a distance of approximately 20 mm from the CMOS. This distance allowed the lens to focus at very close range. The flow cytometer platform, depicted in Figure 2-A, consists of a stationary platform and a moveable stage for focusing. The webcam circuitry and optics were attached to the stationary platform while the flow-cell was attached to the translating stage.

A single video frame of THP-1's stained with SYTO-9 dye in wide-field flow-cell at a flow rate of 500 μL/min is shown in Figure 3-A. The flow-cell geometry and fluorescent detection optics allow for a high signal to noise ratio for easy detection of these cells (Figure 3-B). Compared to a single video frame from flow-focused cell flowing at 1 μL/min (Figure 2-C and 3-D), this suggests that the wide-field cytometer has potential for large volume, high throughput low cell number analysis.

3.3 Wide-field Cytometer Optimization

In order to optimize the performance of a wide-field flow-cell, the volumetric flow rate should be set in accordance with the photodetector characteristics (frame rate, exposure time, and pixel array size). First, the sampling frequency (frame rate) must be determined such that no target cells are able to pass through the sensor field of view (FOV) without being imaged. The residence time (t_R) of a single cell in the imaged FOV is given by

$$t_R = \frac{V_{image}}{\dot{V}}$$

where V_{image} is the volume of fluid visible in the FOV and $\dot{V}$ is the average volumetric flow rate. The maximum frequency with which cells pass through the FOV is then

$$f = \frac{1}{t_R}$$

For the flow to be fully sampled, the sampling rate must be at least twice this value (2*f*). This sets the lower bound of frame rate for the video sensor. The next variable which must be set is the exposure time (t_{EXP}), which has a maximum of $t_R/2$. The image streak length (*SL*) of a single cell is equal to

$$SL = t_{EXP}\frac{L_P}{t_R}$$

where L_P is the length of the flow channel in pixels in the FOV. To minimize streaking without reducing imaged cell intensity, exposure time was set to the time it takes a cell to traverse a single pixel:

$$t_{EXP} = \frac{t_R}{L_P}$$

Because of the approximate Poiseuille flow field present in a flow-cell such as this, cells in the center of the flow will travel at a velocity higher than that expected for the average flow rate (as much as twice the average flow velocity). Settings for frame rates and exposure times may need to be increased in order to compensate for this.

3.4 High throughput Cytometer Performance

To analyze the performance of the wide-field cytometer, human monocytes stained with SYTO-9 dye were analyzed. Figure 4 shows the analysis of a video clip where a single cell moves through the laser spot. Figure 4-A shows a schematic of the primary elements in each video

frame: the flow channel, the laser spot, and the direction of flow. Figure 4-B shows the green channel of a single video frame where no fluorescent cells are present, and Figure 4-C shows a single frame where a single cell (circled) can be seen moving through the flow-cell. In this example, a video clip containing 2,000 frames (10.7 seconds of video) showed a single cell passing through the flow-cell. In order to quickly find a rare event such as this without manually scanning each frame, an image stacking approach was used. The median value and the maximum value of each pixel in the stack of 2,000 frames was calculated. The median image is shown in Figure 4-D, and the maximum image is shown in Figure 4-E with the cell position in each frame marked with an arrow. The median image represents the typical background signal, while the maximum image represents the highest signal recorded at each pixel during the video. In the maximum image, the path taken by a single fluorescent cell can be clearly seen. In order to aide in distinguishing the cell images from background signal, the median image was subtracted from the maximum image to produce Figure 4-F which allows for improved visualization of cell movement. This method of combining multiple video frames was useable for concentrations of cells up to 100 cells/mL. At higher concentrations, the overlap of cell images made it difficult to uniquely identify single cells.

3.5 Counting efficiency for low cell number of the flow cytometer platform

To determine the counting efficiency of this flow cytometer platform the number of cells counted in a particular sample was compared to the number of cells expected. The expected number of cells was determined as described in section 2.5. Figure 5 compares these two values with their respective error margins at concentrations of 100, 10, and 1 cells/mL. The average cell concentrations measured by the flow cytometer at these three respective stock concentrations were 84, 7.9 and 0.56 cells/mL. This suggests that counting efficiency decreased with decreasing concentration. The primary factor which probably contributed to the decreasing counting efficiency at lower concentrations is the performance of the dye. The dye, designed for bacterial staining, was noted to diffuse out of cells over time. The increased time required to prepare and analyze the lower dilutions resulted in the fluorescent signal of some cells to be substantially reduced. Below a certain level these cell images were indistinguishable from noise, and were thus considered to be below the detection threshold of the optical system. The increasing standard deviation evident in lower dilutions is likely due to **stochastic** variation which

causes measurements of cell numbers to fluctuate with greater relative magnitude as the number of cells decreases. Such stochastic variation is clearly shown by the error bars of the measurement of 1 cell/ml in figure 5. More suitable dyes are currently being investigated.

3.6 Counting of labeled THP-1 human monocytes in blood

To determine the counting efficiency of SYTO-9 labeled cells in blood, labeled cells were spiked in blood at a concentration of ~100 cells/mL When analyzing white blood cells, frequently the red blood cells (RBC) are lysed (to avoid interference and to prevent laser absorption) either with ammonium chloride or various commercial whole blood lysing solutions. To avoid the RBC lysis step, we simply diluted the blood by 10X in HEPES buffer, which simplified our protocol while minimizing laser absorption by RBC.

Twenty-two samples of 10X diluted whole blood (3 mL each) spiked to a target concentration of 100 cells/mL (95% CL 93-107 cells/mL) were processed through the wide-field flow cytometer (i.e. 6.6 mL whole blood). Samples were processed through the flow cytometer at a flow rate of 500 μL/min (i.e. a throughput rate of whole blood equal to 50 μL/min). A single image frame is shown in Figure 6-A showing two cells passing through the field of view. The number of fluorescently labeled cells in each sample were counted, and the concentration of cells was calculated. A plot of measured cell concentrations for all twenty-two samples is shown in Figure 6-B. Each data point indicates the number of samples that were found to be within a particular range of concentrations. The average concentration for all samples was determined to be 91.4 cells/mL, with a 95% confidence interval of 86-97 cells/mL. Thus, it appears that the technique provides a reasonably accurate detection of the actual concentration of 100 cells/mL with a tendency towards undercounting the actual concentration by approximately 10%. The results shown in Figure 6-B are similar to those presented in Figure 5 for the data point representing 100 cells/mL. The measured cell concentration in whole blood was 9% less than the calculated expected concentration, but those two values are not significantly different due to the error margins involved. For the data collected in buffer, measured concentration and expected concentration were also not significantly different at the concentration of 100 cells/mL. This

indicates that when whole blood samples are prepared as described here (i.e. diluted 10X), the counting accuracy of the system is accurately represented by experiments conducted in buffer (Figure 5) which enable the detection of ~1cell/ml.

4. CONCLUSIONS

A new simple low-cost flow cytometer based on webcam imaging has been developed that is capable of both high throughput and high sensitivity.

The detection system in this work is based on developing a fluorescence detector for labeled cells. Detection of fluorescently labeled cells is a general method in medical diagnostics. Any cell can be labeled with a cell type-specific fluorescently tagged ligand, and then detected with the fluorescence detector. In previous work, we demonstrated that the fluorescence detector used in this work is capable of sensitive detection of fluorescent signals [13,25-34]. Therefore, this may be a method that can be applied to other fluorescently labeled cells at low cell concentrations.

The flow cytometer was found to be capable of detecting fluorescently tagged cells at concentrations as low as 1 cell/mL at a flow rate of 500 μL/min. These low cell concentrations and the high volume are applicable to rare cell detection such as circulating tumor cell (CTC) analysis. The flow cytometer was realized through the combination of: (1) a webcam capable of 187 frames per second video capture, (2) a 1 W laser module for area-excitation, and (3) a 2D flow-cell that allows for high sample throughput in a wide flow field. This enabled rapid interrogation of the flow field using a linear velocity of target cells that was lower than in the conventional 1D flow-cells typically used in flow cytometry. While mobile phones are commonly used for mobile POC imaging devices, the high flow rate associated with the higher throughput needed for rare cell detection using the new flow cytometer required very high frame rates to avoid streaking and improve image quality. Therefore, a webcam was employed because of its suitable frame rate and low cost (e.g. $30).

The sensitivity and throughput of this webcam-based flow cytometer with wide-field imaging was then investigated using THP-1 human monocytes stained with SYTO-9 dye in the 2D flow-cell was analyzed in blood and in buffer. For blood spiked to 100 cells/ml, average concentration for all samples was 91.4 cells/mL, with a 95% confidence interval of 86-97 cells/mL.

Measurements were made at concentrations of 100, 10, and 1 cells/mL, and compared with manual counting in a microscope. The average counting efficiency at these three concentrations was found to be 84%, 79% and 56%, respectively. The lower counting efficiency at the lowest concentrations is probably because of the dye diffusion, so the cells are more difficult to identify and distinguish from noise, for such cells the signal may be below the detection threshold of the optical system. The results of counting fluorescently labeled THP-1 monocytes spiked into whole blood and the distribution of cell counts from 22 samples suggest that counting accuracy in blood is accurately represented by experiments conducted in buffer.

These efficiencies are suitable for rare cell detection, though there is room for improvement at very low concentration. The simplicity and the low cost of the webcam flow cytometer suggests that this configuration may have the potential for developing POC clinical flow cytometry for resource-poor settings associated with global health.

FIGURE LEGENDS

Figure 1 – Webcam-based flow focusing cytometry. (I) A schematic of the flow focusing cell shown with key structures: A) sample inlet, B) sheath fluid inlets, C) interrogation region, D) waste outlet. (II) A schematic of the flow focusing interrogation region with features labeled E) focused sample stream (food dye used for visualization), F) sheath fluid, G) channel boundary. (III) A photograph of flow focusing. (IV) An image of flow-focused 5 μm polystyrene beads, (V) 3D representation of image signal from IV.

Figure 2 – Schematic of webcam-based wide-field flow cytometer – (A) The wide-field flow cytometer consists of four modules: a sensing element, excitation source, flow-cell, and a stage to hold each module in alignment. The sensing element consists of the internal elements of a webcam, a 12 mm f/1.2 CCTV lens, a green emission filter, and a computer to collect and analyze data. The excitation source is a 450 nm 1W laser module. The sample handling module consists of a flow-cell and a programmable syringe pump. (B) A schematic of the wide-field flow-cell with key elements labeled.

Figure 3 A comparison between webcam-based wide-field flow cytometer and webcam-based flow focusing cytometry A) single video frame of THP-1 human monocytes labeled with SYTO-9 in wide-field flow-cell at 500 μL/min, B) 3D visualization of A, C) single video frame of polystyrene beads in flow-focused cell at 1 μL/min, D) 3D visualization of C.

Figure 4 – Analysis of a single cell using webcam-based wide-field flow cytometry (single cell moving through laser spot). (A) Schematic of webcam field of view showing flow channel, elliptical laser illumination spot and flow direction, (B) single raw video frame showing no fluorescent THP-1's present, (C) single frame showing one THP-1 cell labeled with SYTO-9, (D) median pixel value from 2000 frames showing average background autofluorescence from flow-cell, (E) maximum pixel value from 2000 video frames showing a single cell moving through the laser spot (marked with arrows), (F) result of subtracting image D from image E, allowing for improved visualization of cell movement and faint cell images.

Figure 5 – Webcam-based wide-field flow cytometer counting efficiency. Results of three concentrations of human monocytes labeled with SYTO-9 counted manually (light grey fill) and using the webcam-based flow cytometer (dark grey fill). Error bars represent standard error for each data set. Manual counting was performed at a higher stock concentration (1000 cells/mL) and the results for each target concentration were calculated.

Figure 6 – Counting fluorescently labeled THP-1 monocytes spiked into whole blood. SYTO-9 Labeled THP-1 monocytes were labeled and spiked into whole blood to a target concentration of 100 cells/mL (95% CL 93-107 cells/mL). The blood samples were diluted 10X in HEPES buffer to prevent laser absorption by red blood, and counted with webcam-based wide-field flow cytometer. **(**A) typical image frame from the flow cytometer capable of detecting multiple cells in the field (two circled). (B) A histogram of measured cell concentration of 22 samples counted using the flow cytometer, which indicated a Poisson's distribution (dotted line) for the measurements with an average of 91.4 cells/mL (95% CL 86-97 cells/mL).

REFERENCES

1. J. P. Golden, J. S. Kim, J. S. Erickson, L. R. Hilliard, P. B. Howell, G. P. Anderson, M. Nasir and F. S. Ligler, *Lab on a chip*, 2009, **9**, 1942-1950.
2. P. B. Howell, Jr., J. P. Golden, L. R. Hilliard, J. S. Erickson, D. R. Mott and F. S. Ligler, *Lab on a chip*, 2008, **8**, 1097-1103.
3. E. K. Zuba-Surma and M. Z. Ratajczak, *Methods Cell Biol*, 2011, **102**, 207-230.
4. T. C. George, D. A. Basiji, B. E. Hall, D. H. Lynch, W. E. Ortyn, D. J. Perry, M. J. Seo, C. A. Zimmerman and P. J. Morrissey, *Cytometry A*, 2004, **59**, 237-245.
5. P. V. Beum, M. A. Lindorfer, B. E. Hall, T. C. George, K. Frost, P. J. Morrissey and R. P. Taylor, *Journal of immunological methods*, 2006, **317**, 90-99.
6. N. Lopez-Riquelme, A. Minguela, F. Villar-Permuy, D. Ciprian, A. Castillejo, M. R. Alvarez-Lopez and J. L. Soto, *APMIS : acta pathologica, microbiologica, et immunologica Scandinavica*, 2013.
7. C. R. Taitt, G. P. Anderson and F. S. Ligler, *Biosens Bioelectron*, 2005, **20**, 2470-2487.
8. M. M. Ngundi, S. A. Qadri, E. V. Wallace, M. H. Moore, M. E. Lassman, L. C. Shriver-Lake, F. S. Ligler and C. R. Taitt, *Environmental science & technology*, 2006, **40**, 2352-2356.
9. M. C. Moreno-Bondi, C. R. Taitt, L. C. Shriver-Lake and F. S. Ligler, *Biosens Bioelectron*, 2006, **21**, 1880-1886.
10. F. S. Ligler, K. E. Sapsford, J. P. Golden, L. C. Shriver-Lake, C. R. Taitt, M. A. Dyer, S. Barone and C. J. Myatt, *Anal Sci*, 2007, **23**, 5-10.
11. Y. Kostov, N. Sergeev, S. Wilson, K. E. Herold and A. Rasooly, *Methods Mol Biol*, 2009, **503**, 259-272.
12. K. E. Sapsford, S. Sun, J. Francis, S. Sharma, Y. Kostov and A. Rasooly, *Biosens Bioelectron*, 2008, **24**, 618-625.
13. S. Sun, J. Francis, K. E. Sapsford, Y. Kostov and A. Rasooly, *Sensors and actuators. B, Chemical*, 2010, **146**, 297-306.
14. S. Sun, M. Ossandon, Y. Kostov and A. Rasooly, *Lab on a chip*, 2009, **9**, 3275-3281.
15. S. Sun, M. Yang, Y. Kostov and A. Rasooly, *Lab on a chip*, 2010, **10**, 2093-2100.
16. H. Zhu and A. Ozcan, *Journal of visualized experiments : JoVE*, 2013.
17. H. Zhu, S. Mavandadi, A. F. Coskun, O. Yaglidere and A. Ozcan, *Anal Chem*, 2011, **83**, 6641-6647.
18. Q. Wei, H. Qi, W. Luo, D. Tseng, S. J. Ki, Z. Wan, Z. Gorocs, L. A. Bentolila, T. T. Wu, R. Sun and A. Ozcan, *ACS nano*, 2013, **7**, 9147-9155.
19. A. F. Coskun, R. Nagi, K. Sadeghi, S. Phillips and A. Ozcan, *Lab on a chip*, 2013, **13**, 4231-4238.
20. I. Navruz, A. F. Coskun, J. Wong, S. Mohammad, D. Tseng, R. Nagi, S. Phillips and A. Ozcan, *Lab on a chip*, 2013, **13**, 4015-4023.
21. H. Zhu, I. Sencan, J. Wong, S. Dimitrov, D. Tseng, K. Nagashima and A. Ozcan, *Lab on a chip*, 2013, **13**, 1282-1288.
22. H. Zhu, U. Sikora and A. Ozcan, *Analyst*, 2012, **137**, 2541-2544.
23. H. Zhu, O. Yaglidere, T. W. Su, D. Tseng and A. Ozcan, *Conference proceedings : ... Annual International Conference of the IEEE Engineering in Medicine and Biology*

Society. IEEE Engineering in Medicine and Biology Society. Conference, 2011, **2011**, 6801-6804.
24. H. Zhu, O. Yaglidere, T. W. Su, D. Tseng and A. Ozcan, *Lab on a chip*, 2011, **11**, 315-322.
25. J. Balsam, R. Rasooly, H. A. Bruck and A. Rasooly, *Biosens Bioelectron*, 2014, **51**, 1-7.
26. A. Rasooly, Y. Kostov and H. A. Bruck, *Methods Mol Biol*, 2013, **949**, 365-385.
27. A. Rasooly, H. A. Bruck and Y. Kostov, *Methods Mol Biol*, 2013, **949**, 451-471.
28. J. Balsam, H. A. Bruck and A. Rasooly, *Methods*, 2013, **63**, 276-281.
29. J. Balsam, H. A. Bruck and A. Rasooly, *Sensors and actuators. B, Chemical*, 2013, **186**, 711-717.
30. J. Balsam, M. Ossandon, H. A. Bruck and A. Rasooly, *Analyst*, 2012, **137**, 5011-5017.
31. J. Balsam, H. A. Bruck, Y. Kostov and A. Rasooly, *Sensors and actuators. B, Chemical*, 2012, **171-172**, 141-147.
32. M. Yang, S. Sun, Y. Kostov and A. Rasooly, *Sensors and actuators. B, Chemical*, 2011, **153**, 176-181.
33. J. Balsam, M. Ossandon, Y. Kostov, H. A. Bruck and A. Rasooly, *Lab on a chip*, 2011, **11**, 941-949.
34. K. E. Sapsford, J. Francis, S. Sun, Y. Kostov and A. Rasooly, *Anal Bioanal Chem*, 2009, **394**, 499-505.
35. J. Balsam, M. Ossandon, H. A. Bruck, I. Lubensky and A. Rasooly, *Expert opinion on medical diagnostics*, 2013, **7**, 243-255.

Figure 1

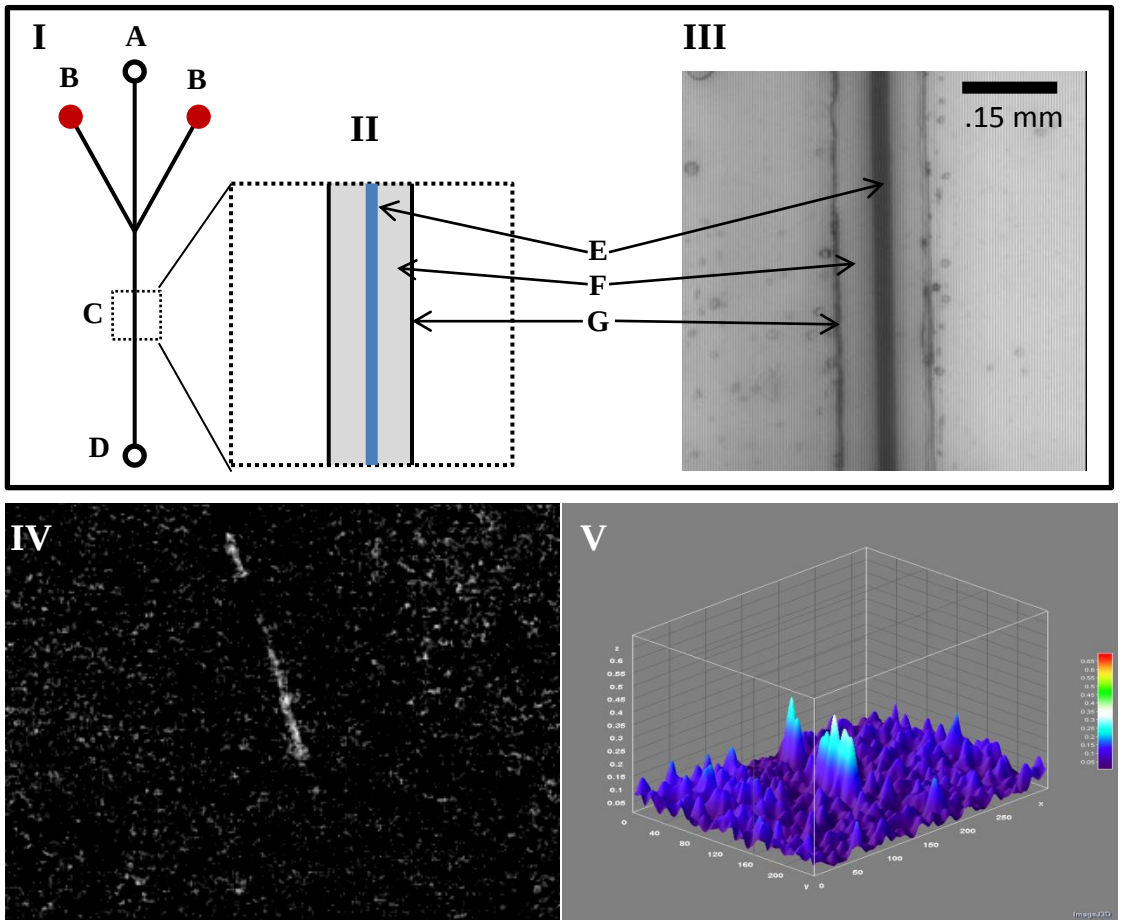

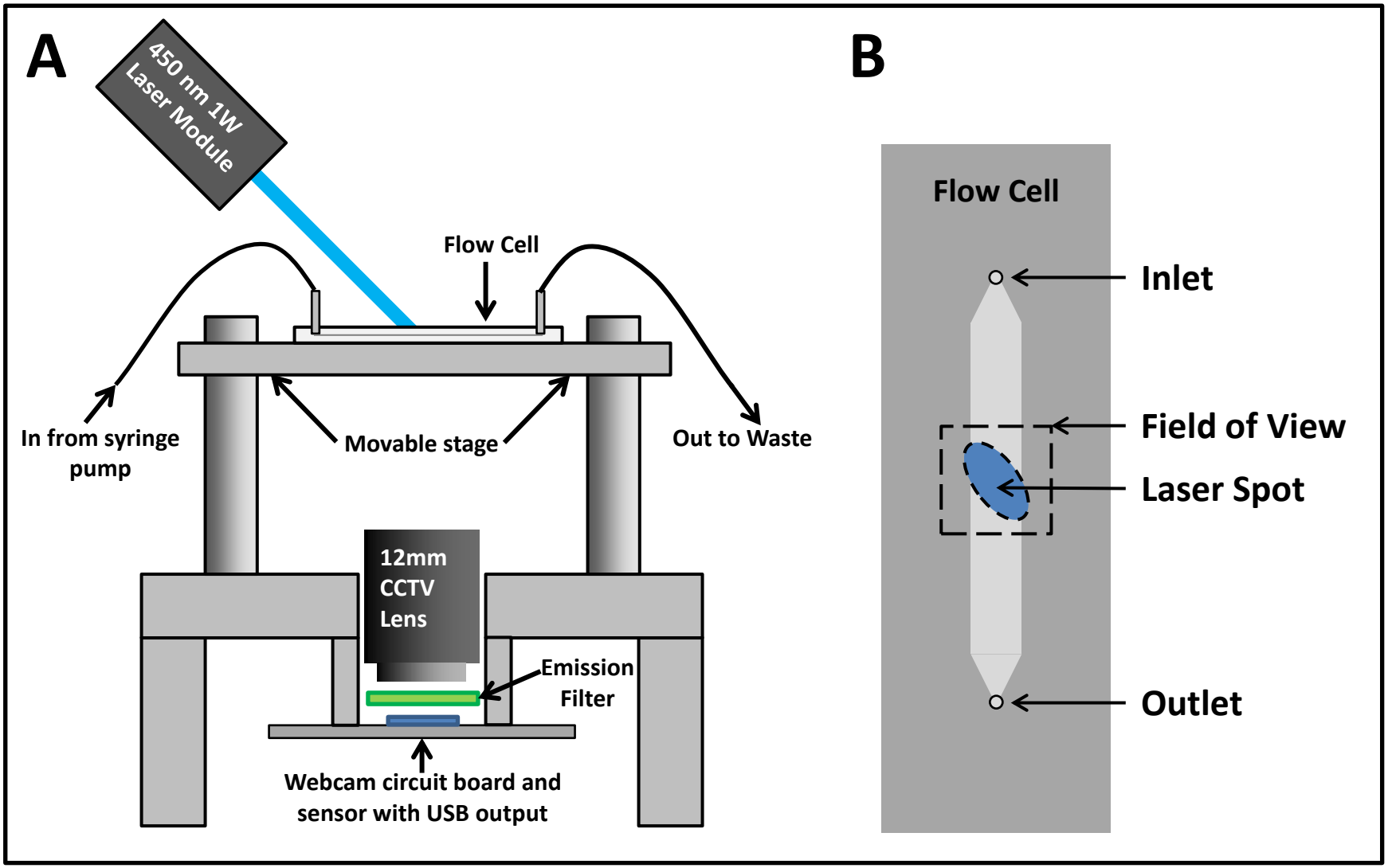

Figure 3

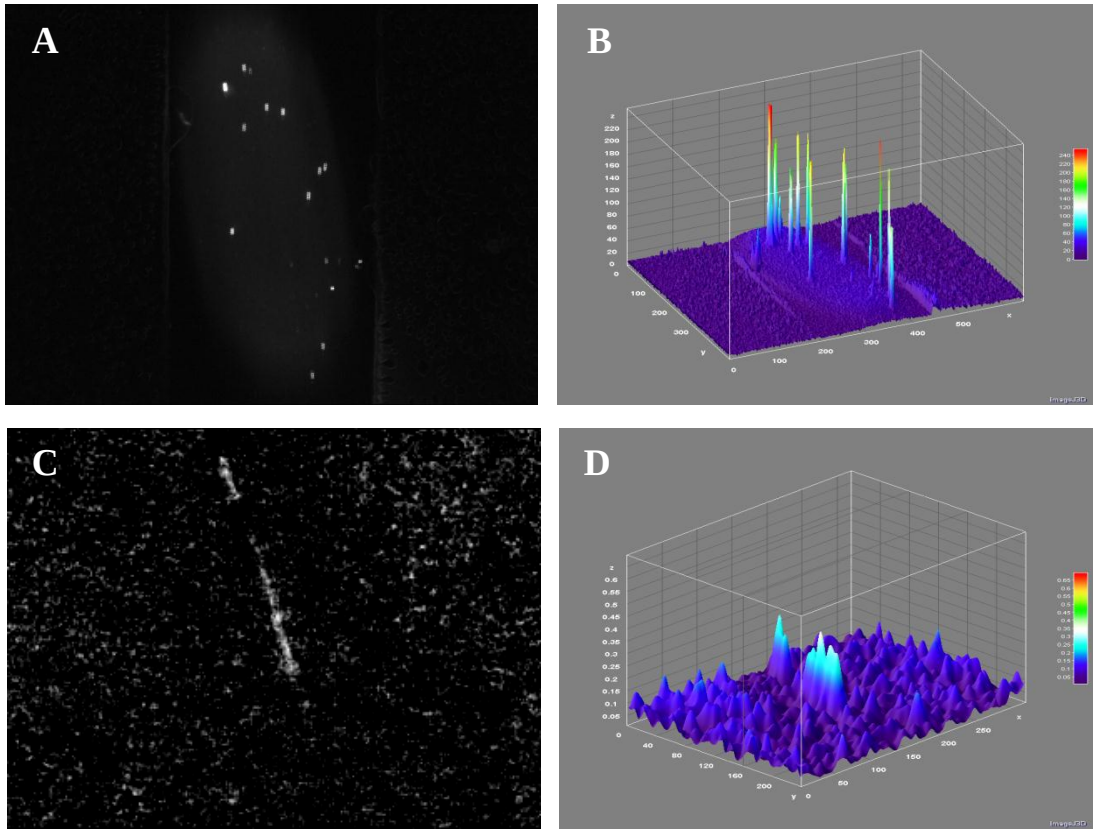

Figure 4

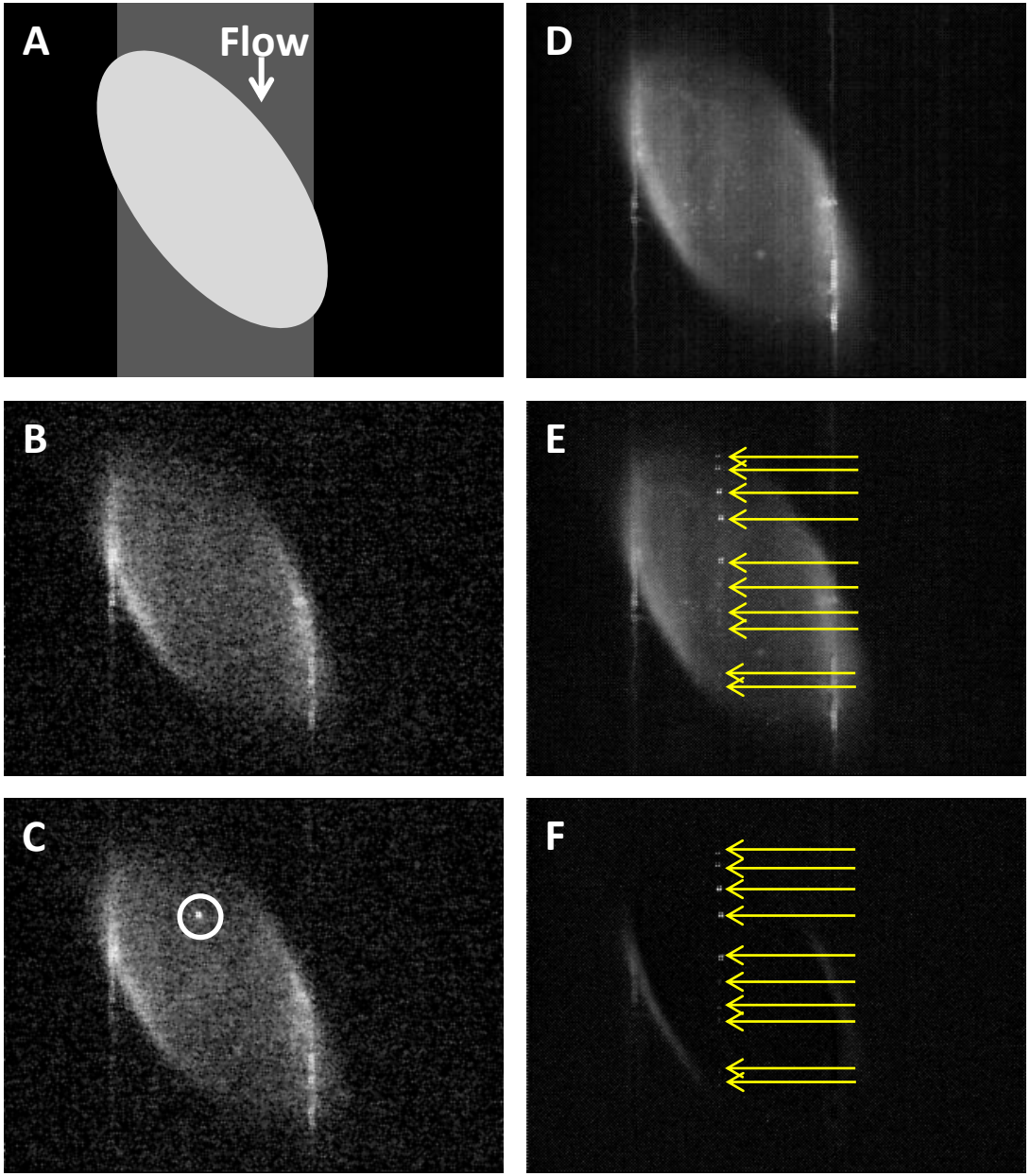

Figure 5

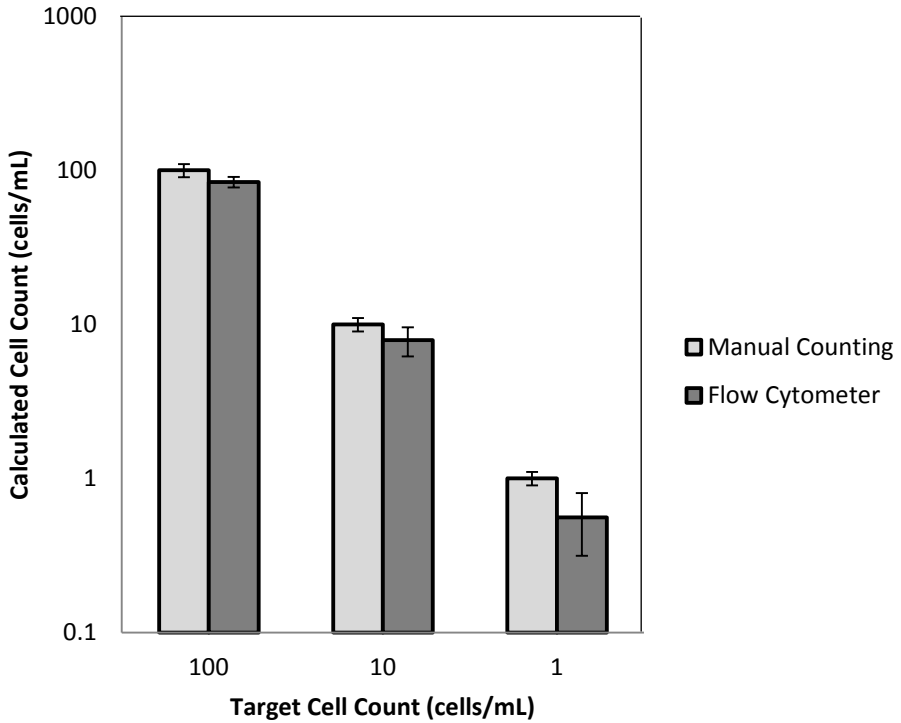

Figure 6